Patterns of $\alpha_v\beta_3$ Expression in Primary and Metastatic Human Breast Cancer as Shown by ^{18}F-Galacto-RGD PET

Ambros J. Beer[1], Markus Niemeyer[2], Janette Carlsen[1], Mario Sarbia[3], Jörg Nährig[3], Petra Watzlowik[1], Hans-Jürgen Wester[1], Nadia Harbeck[2], and Markus Schwaiger[1]

[1]Department of Nuclear Medicine, Klinikum rechts der Isar, Technische Universität München, Munich, Germany; [2]Department of Gynecology, Klinikum rechts der Isar, Technische Universität München, Munich, Germany; and [3]Department of Pathology, Klinikum rechts der Isar, Technische Universität München, Munich, Germany

The integrin $\alpha_v\beta_3$ is a key player in angiogenesis and metastasis. Our aim was to study the uptake patterns of the $\alpha_v\beta_3$-selective PET tracer ^{18}F-galacto-RGD in invasive ductal breast cancer. **Methods:** Sixteen patients with primary ($n = 12$) or metastasized breast cancer ($n = 4$) were examined with ^{18}F-galacto-RGD PET. Standardized uptake values (SUVs) were derived by region-of-interest analysis, and immunohistochemistry of $\alpha_v\beta_3$ expression was performed ($n = 5$). **Results:** ^{18}F-Galacto-RGD PET identified all invasive carcinomas, with SUVs from 1.4 to 8.7 (mean ± SD, 3.6 ± 1.8; tumor-to-blood and tumor-to-muscle ratios, 2.7 ± 1.6 and 6.2 ± 2.2, respectively). Lymph-node metastases were detected in 3 of 8 patients (mean SUV, 3.3 ± 0.8). SUVs in distant metastases were heterogeneous (2.9 ± 1.4). Immunohistochemistry confirmed $\alpha_v\beta_3$ expression predominantly on microvessels (5/5) and, to a lesser extent, on tumor cells (3/5). **Conclusion:** Our results suggest generally elevated and highly variable $\alpha_v\beta_3$ expression in human breast cancer lesions. Consequently, further imaging studies with ^{18}F-galacto-RGD PET in breast cancer patients for assessment of angiogenesis or planning of $\alpha_v\beta_3$-targeted therapies are promising.

Key Words: breast cancer; integrins; $\alpha_v\beta_3$; angiogenesis; PET; RGD

J Nucl Med 2008; 49:255–259
DOI: 10.2967/jnumed.107.045526

The treatment of breast cancer nowadays requires an individualized approach and determination of the best therapeutic strategy. The integrin $\alpha_v\beta_3$ is an interesting target for specific therapies in oncology and as a new prognostic factor, as it is highly expressed on activated endothelial cells during angiogenesis and plays an important role in the regulation of tumor growth, local invasiveness, and metastatic potential (*1–3*). Specifically in breast cancer, its involvement in metastasis, and especially in migration of tumor cells to the bone, has been demonstrated in preclinical tumor models (*4,5*). Moreover, anti-$\alpha_v\beta_3$–targeted drugs, alone or in combination with radioimmunotherapy, have been proven to be effective in breast cancer xenografts (*6,7*). Histopathologic studies have examined the role of integrin $\alpha_v\beta_3$ in human breast cancer and have shown contradicting results (*8–11*). Molecular imaging has the potential to show specific biologic properties of tissues as a whole and also in several tumor sites in the body in one session (*12*). Therefore, imaging of $\alpha_v\beta_3$ expression might help to elucidate the complex role of this integrin in human breast cancer patients. We have developed the $\alpha_v\beta_3$-specific tracer ^{18}F-galacto-RGD for PET (*13*). It has already been demonstrated that ^{18}F-galacto-RGD PET allows specific imaging of $\alpha_v\beta_3$ expression and that the uptake of ^{18}F-galacto-RGD correlates with $\alpha_v\beta_3$ expression in tumor xenografts as well as in patients (*14–17*). We now report—to our knowledge, for the first time—on the specific use of ^{18}F-galacto-RGD PET in breast cancer patients. The goals of our study were to analyze the uptake patterns of ^{18}F-galacto-RGD in normal breast tissue and in primary as well as metastatic tumor lesions. Our hypothesis was that ^{18}F-galacto-RGD PET allows for identification of $\alpha_v\beta_3$ expression in primary and metastatic breast cancer lesions with good image quality, which, in consequence, would demonstrate its usefulness for future applications such as noninvasive assessment of angiogenesis and integrin $\alpha_v\beta_3$ expression in human breast cancer.

MATERIALS AND METHODS

Radiopharmaceutical Preparation

Synthesis of the labeling precursor and subsequent ^{18}F labeling were performed as described previously (*18*).

Patients

The study was approved by the Ethics Committee of the Technische Universität München, and informed written consent was obtained from all patients. Sixteen patients were included in the study (15 female, 1 male; mean age ± SD, 62.1 ± 11.7 y).

Received Jul. 20, 2007; revision accepted Oct. 12, 2007.
For correspondence or reprints contact: Ambros J. Beer, MD, Department of Nuclear Medicine, Klinikum rechts der Isar, Technische Universität München, Ismaninger Strasse 22, 81675 Munich, Germany.
E-mail: beer@roe.med.tum.de

Inclusion criteria consisted of:

- Either biopsy-proven or suspected primary breast cancer (Breast Imaging Reporting and Data System [BIRADS] 4 or 5) according to conventional staging (mammography and breast ultrasound, chest radiography, ultrasound of abdomen and bone scintigraphy; additional MRI mammography in 5 patients);
- Size of primary lesions scheduled for surgery of at least 1.5 cm in maximum diameter as determined by conventional imaging because of the limited resolution of PET;
- Known metastasized breast cancer according to clinical staging (bone scintigraphy and CT in all patients; ^{18}F-FDG PET/CT in 1 patient);
- Age $>$ 18 y;
- Ability to give written and informed consent.

Exclusion criteria consisted of pregnancy, lactation period, and impaired renal function (serum creatinine level $>$ 1.2 mg/dL).

For details on the patient population, see Table 1.

PET Procedure

Imaging was performed with an ECAT EXACT PET scanner (Siemens Medical Solutions, Inc.) as described previously (*17*). In each subject, a static emission scan was acquired in the caudocranial direction, beginning on average 63.0 ± 4.1 min (mean ± SD) after injection of ^{18}F-galacto-RGD, covering a field of view at least from the pelvis to the thorax (5–7 bed positions, 5 min per bed position). The imaging time point was chosen according to former results from dynamic and serial static emission scans, showing good tumor-to-background contrast ~60 min after injection (*14*).

Image Analysis

Positron emission data were reconstructed using the ordered-subsets expectation maximization (OSEM) algorithm using 8 iterations and 4 subsets. The images were corrected for attenuation using the collected transmission data. For image analysis, CAPP software, version 7.1 (Siemens Medical Solutions, Inc.), was used. The static emission scans were calibrated to standardized uptake values (SUVs).

In the static emission scans, circular regions of interest (ROIs) with a diameter of 1.5 cm were placed over the left ventricle, the forearm (muscle tissue activity), breast tissue on the contralateral side to the tumor-bearing breast, liver, spleen, lung, and tumor tissue in 3 adjacent slices by an experienced operator. Polygonal free-hand ROIs were placed over the intestine in areas with visible tracer uptake in the lower abdomen. Results were expressed in mean SUV. In the tumors, the areas with the maximum intensity were chosen for measurements. In tumors with a diameter of ≤2 cm and visible uptake ($n = 4$), the SUV might be underestimated because of partial-volume effects. Therefore, the diameter of the ROI was adapted to the tumor size, and the SUV in the ROI was corrected for partial-volume effects using the tumor diameter mentioned in the pathology report and the correction tables established by Brix et al. for our PET scanner by phantom studies (*19*).

For evaluation of the sensitivity of ^{18}F-galacto-RGD for primary staging, lesions with elevated uptake on ^{18}F-galacto-RGD PET were compared with the results of conventional staging, and

TABLE 1
Patient Data

Patient no.	Age (y)	TNM stage	Tu size (cm)	SUV Tu	SUV LN	SUV Met	Staining pattern IHC $\alpha_v\beta_3$
1	73	pT2 pN1a pMXR0	4.0	3.6	Neg.	—	Tumor cells and vessels positive, moderate
2	38	ypT0 N0 M0	NA*	NA*	NA*	NA*	
3	64	pT3 pN3a pMXR0	3.0	4.3	Neg.	—	Tumor cells and vessels positive, intense
4	63	pT2m pN3a MXR0	4.5	2.5	2.2	—	Tumor vessels positive, weak
			1.5	1.5			
5	73	pT2 pN0 MXR0	4.0	8.7	—	—	Tumor cells and vessels positive, intense
6	40	NA†	—	—	—	—	
7	73	pT2 pN2a pMXR0	2.0	3.0	Neg.	—	
8	68	pT2 pN0 MXR1	2.1	3.1	—	—	
9	70	pT4b pN2a(4/5) cM1R1	6.0	3.6	3.5	3.8 1.2	
10	70	cT4c N2c M1	4.0	4.1	4.1	3.1	Tumor vessels positive, weak
11	68	pT1c pN1(sn1/1) pMX	1.6	2.8	Neg.	—	
12	44	pT4b N3a MXR0	4.5	3.2	Neg.	—	
13	54	pT3c N0 M1	2.0	3.8	—	2.8 3.0	
14	66	pT3c N2c M1	—	—	—	2.2 3.0 3.3	
15	68	pT4c N1 M0	7.0	2.3	—	—	
16	65	pT2m N1 M1biv	NA	NA	NA	2.6	

*No viable tumor cells found after neoadjuvant chemotherapy.

†Tumor suspected according to MR mammography (BIRADS 4), no tumor histopathologically.

Tu size = maximum tumor diameter (cm); SUV Tu, SUV LN, and SUV Met = tracer uptake as standardized uptake value (SUV) in tumors, lymph nodes, and distant metastases; IHC $\alpha_v\beta_3$ = immunohistochemistry with $\alpha_v\beta_3$-specific antibody LM609; Neg. = negative; NA = not applicable.

histopathologic staging served as the standard of reference. For evaluation of metastatic lesions, the findings of clinical staging served as the standard of reference. A maximum of 10 lesions was evaluated per patient, as 2 patients had disseminated metastatic disease to the liver and bone.

Collection of Tissue Samples and Immunohistochemistry of $\alpha_v\beta_3$ Expression

The mean time interval between PET and surgery was 2.4 ± 2.3 d. In the operating room, tissue samples from the tumors were obtained from tumor regions with maximum tracer uptake. The specimens were snap-frozen in liquid nitrogen and stored at −70°C until staining was performed.

For immunohistochemical investigation, frozen tumor tissues were sectioned (6 μm) and stained using the biotinylated monoclonal anti-$\alpha_v\beta_3$ antibody LM609 (1:100; Chemicon Europe). Sections were processed by peroxidase staining (peroxidase substrate AEC [3-amino-9-ethylcarbazole] kit; Vector Laboratories).

Analysis of staining of microvessel and tumor cells was performed by a senior pathologist, who was unaware of the results of the SUV measurements.

Statistical Analysis

All quantitative data are expressed as mean ± 1 SD. The correlation between quantitative parameters was evaluated by linear regression analysis and by calculation of the Pearson correlation coefficient *R*. Statistical significance was tested by using ANOVA. All statistical tests were performed at the 5% level of statistical significance, using MedCalc statistical software (version 6.15.000).

RESULTS

Static Emission Scans

During the observation period of ~3 h after tracer injection until the end of scanning, no adverse reactions were noted in our patient population.

The results of the SUV measurements are summarized in Figure 1. The mean tumor-to-blood ratio was 2.9 ± 1.7, and the mean tumor-to-muscle ratio was 6.6 ± 1.9. The SUVs of the primary tumors (n = 12) did not correlate with the tumor diameter (r = 0.116, P = 0.719).

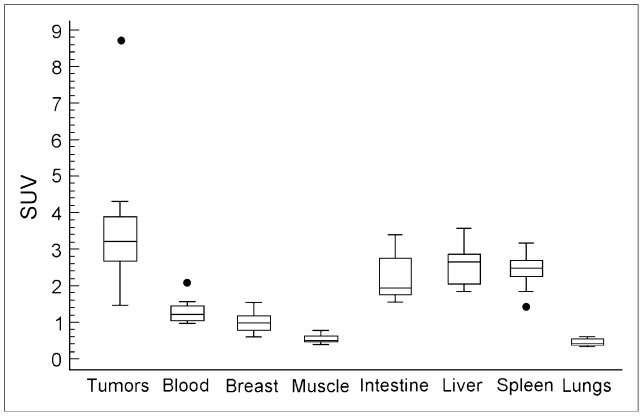

FIGURE 1. Box plot diagram of mean SUVs of tumors and normal tissue (breast, muscle, blood pool, liver, spleen, lungs, intestine) from static emission scans. Tumor uptake was very heterogeneous but higher than uptake in background tissue, resulting in good image contrast.

Comparison with Clinical Staging

In the static emissions scans, all primary tumors could be identified (n = 12/12). No false-positive findings occurred in the tumor-bearing or the contralateral breast. One patient was scanned after completion of neoadjuvant chemotherapy with no residual viable tumor cells in histology (ypT0) and no elevated signal on the ^{18}F-galacto-RGD PET scan. One patient with a suggestive finding according to mammography and MRI mammography (BIRADS 4) showed no elevated uptake on the ^{18}F-galacto-RGD PET scan, and no tumor was found on histopathology. Lymph-node metastases were detected in 3 of 8 patients with a mean SUV of 3.3 ± 0.8. Although the mean size of the missed metastases was small—5.8 ± 7.2 mm—not only microscopic but also macroscopic lymph-node metastases were missed (size, 15 and 20 mm). Eleven of 24 evaluated distant metastases were detected by ^{18}F-galacto-RGD PET and SUVs were heterogeneous (mean, 2.9 ± 1.4; range, 1.0–3.8). Osseous metastases were depicted successfully by ^{18}F-galacto-RGD PET on a per-patient basis (n = 4); however, some osseous metastases in the same patients did not show tracer uptake. Also, multiple metastases to the liver were not identified in 1 patient. One small lung lesion was detected by ^{18}F-galacto-RGD PET, which was not detected by conventional staging, and which was confirmed by CT (Fig. 2).

Immunohistochemistry of $\alpha_v\beta_3$ Expression

$\alpha_v\beta_3$ expression could be confirmed by immunohistochemistry in all tumor specimens. $\alpha_v\beta_3$ expression was identified predominantly on the endothelium of newly formed blood vessels. In 3 specimens, $\alpha_v\beta_3$ expression could also be seen on the tumor cells themselves in addition to staining of the neovasculature (Fig. 3).

DISCUSSION

In this study we could demonstrate elevated but highly variable $\alpha_v\beta_3$ expression in primary and metastatic breast cancer by using ^{18}F-galacto-RGD and PET, with the integrin being expressed predominantly on endothelial cells and, to a lesser extent, on tumor cells. ^{18}F-Galacto-RGD PET performed well for primary tumor detection but did not show sufficient sensitivity for lymph-node staging.

Our results demonstrated ^{18}F-galacto-RGD uptake in all primary tumor lesions, which was very heterogeneous and did not depend on tumor size. Tracer uptake in metastases also was very heterogeneous. This suggests generally elevated but widely varying levels of $\alpha_v\beta_3$ expression in human breast cancer. This information contributes to the growing literature about integrin expression in human breast cancer, as results from former histopathologic studies were contradictory (*8,11*). Up to now, only 1 other study has examined $\alpha_v\beta_3$ expression in humans with imaging methods using the $\alpha_v\beta_3$-specific SPECT (single-photon CT) tracer ^{99m}Tc-

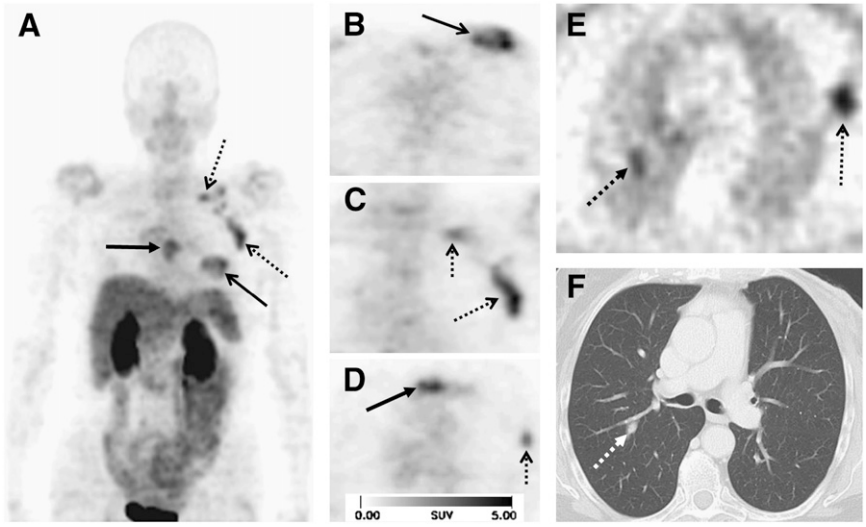

FIGURE 2. A 70-y-old patient with invasive ductal breast cancer of left breast (arrow, open tip), axillary lymph-node metastases on left side (arrow, open tip, dotted line), an osseous metastasis to the sternum (arrow, closed tip), and a pulmonary metastasis on right side (arrow, closed tip, dotted line). Maximum-intensity projection of ^{18}F-galacto-RGD PET (A) and planar images (B, axial plane; C, coronal plane; D, axial plane) show primary tumor, lymph-node metastases, and osseous metastasis with good tumor-to-background contrast. High tracer retention is notable in urogenital tract, predominantly due to renal tracer elimination. Intermediate uptake is notable in liver, spleen, and intestine. One small pulmonary lesion was notable in nonattenuation–corrected images (E) and confirmed by CT (F). In the context of metastasized breast cancer, this was considered to be highly suggestive of a pulmonary metastasis.

NC100692 (*20*). Our results illustrate that noninvasive imaging of $\alpha_v\beta_3$ expression with PET is feasible with good quality in breast cancer patients. However, the small number of patients studied is a limitation, and further prospective studies using ^{18}F-galacto-RGD in a larger patient population to evaluate the biologic and clinical significance of this tracer in more detail are warranted.

The immunohistochemistry of $\alpha_v\beta_3$ expression in primary tumors in our study revealed $\alpha_v\beta_3$ expression predominantly on endothelial cells as well as on tumor cells. Therefore, the signal from ^{18}F-galacto-RGD PET represents a mixture of tracer binding on neovasculature and on tumor cells. This is in accordance with clinical as well as preclinical reports that describe $\alpha_v\beta_3$ expression on neovasculature and on breast cancer cells (*8*). Consequently, $\alpha_v\beta_3$ imaging for assessment of angiogenesis alone should be interpreted carefully in the context of breast cancer as part of the signal might be attributed to tumor cells and not to neovasculature alone. Quantification of $\alpha_v\beta_3$ expression in tumor specimens and correlation with tracer uptake was not performed because of the low number of samples, which is a limitation of our study. However, a significant correlation of $\alpha_v\beta_3$ expression in immunohistochemistry and ^{18}F-galacto-RGD uptake has been demonstrated previously in murine tumor models as well as in patients using static emission scans such as in the current study (*16,17*).

^{18}F-Galacto-RGD PET also showed good results relating to the identification of primary lesions with no false-positive results in breast cancer. However, it must be noted that only lesions with a diameter of 15 mm or larger were included in

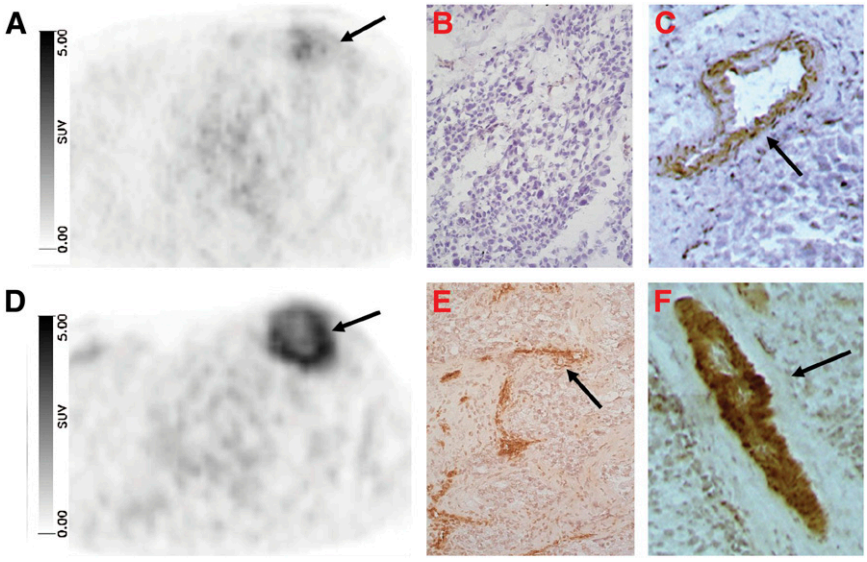

FIGURE 3. Comparison of ^{18}F-galacto-RGD PET (A and D) and immunohistochemistry of $\alpha_v\beta_3$ expression (B, C, E, and F). (Upper row) Patient with large invasive ductal carcinoma of left breast and low ^{18}F-galacto-RGD uptake (A, arrow). Corresponding immunohistochemistry shows negative staining of most parts of tumor (C, low magnification) and only faint positive staining of single vessels (D, high magnification; arrow). (Lower row) Patient with invasive ductal carcinoma of left breast and intense ^{18}F-galacto-RGD uptake (D, arrow). Corresponding immunohistochemistry (E, low magnification; F, high magnification) shows intense staining of tumor vessels (arrow).

our study, because visualization of smaller lesions might be problematic due to the limited resolution of a clinical PET scanner, which is in the range of 5–6 mm (*12*). Moreover, primarily invasive ductal carcinomas were examined in our study, so no conclusions can be drawn about the efficacy of ^{18}F-galacto-RGD PET for imaging of lobular carcinoma. The sensitivity for lymph-node metastases or distant metastases in our small patient sample was not adequate for use in N or M staging in clinical routine. This still must be evaluated in more detail in future comparative studies.

CONCLUSION

Imaging of $\alpha_v\beta_3$ expression in invasive ductal breast cancer with ^{18}F-galacto-RGD PET is possible with good image quality, with $\alpha_v\beta_3$ expression being elevated but highly variable in primary tumors as well as in metastases.

ACKNOWLEDGMENTS

We thank the Cyclotron and PET team—especially Michael Herz, Gitti Dzewas, Coletta Kruschke, and Nicola Henke for excellent technical assistance—and the Münchner Medizinische Wochenschrift and the Sander Foundation for financial support.

REFERENCES

1. Hood JD, Cheresh DA. Role of integrins in cell invasion and migration. *Nat Rev Cancer.* 2002;2:91–100.
2. Ruoslahti E. Specialization of tumor vasculature. *Nat Rev Cancer.* 2002;2:83–90.
3. Brooks PC, Clark RAF, Cheresh DA. Requirement of vascular integrin $\alpha_v\beta_3$ for angiogenesis. *Science.* 1994;2674:569–571.
4. Rolli M, Fransvea E, Pilch J, Saven A, Felding-Habermann B. Activated integrin alpha$_v$beta$_3$ cooperates with metalloproteinase MMP-9 in regulating migration of metastatic breast cancer cells. *Proc Natl Acad Sci USA.* 2003;100:9482–9487.
5. Liapis H, Flath A, Kitazawa S. Integrin alpha$_v$beta$_3$ expression by bone-residing breast cancer metastases. *Diagn Mol Pathol.* 1996;5:127–135.
6. Brooks PC, Stromblad S, Klemke R, Visscher D, Sarkar FH, Cheresh DA. Antiintegrin alpha$_v$beta$_3$ blocks human breast cancer growth and angiogenesis in human skin. *J Clin Invest.* 1995;96:1815–1822.
7. Burke PA, DeNardo SJ, Miers LA, Lamborn KR, Matzku S, DeNardo GL. Cilengitide targeting of alpha$_v$beta$_3$ integrin receptor synergizes with radioimmunotherapy to increase efficacy and apoptosis in breast cancer xenografts. *Cancer Res.* 2002;62:4263–4272.
8. Gasparini G, Brooks PC, Biganzoli E, et al. Vascular integrin alpha$_v$beta$_3$: a new prognostic indicator in breast cancer. *Clin Cancer Res.* 1998;4:2625–2634.
9. Damjanovich L, Fulop B, Adany R, Nemes Z. Integrin expression on normal and neoplastic human breast epithelium. *Acta Chir Hung.* 1997;36:69–71.
10. Pignatelli M, Cardillo MR, Hanby A, Stamp GW. Integrins and their accessory adhesion molecules in mammary carcinomas: loss of polarization in poorly differentiated tumors. *Hum Pathol.* 1992;23:1159–1166.
11. Berry MG, Gui GP, Wells CA, Carpenter R. Integrin expression and survival in human breast cancer. *Eur J Surg Oncol.* 2004;30:484–489.
12. Weber WA. Positron emission tomography as an imaging biomarker. *J Clin Oncol.* 2006;24:3282–3292.
13. Haubner R, Wester HJ, Weber WA, et al. Noninvasive imaging of alpha$_v$beta$_3$ integrin expression using ^{18}F-labeled RGD-containing glycopeptide and positron emission tomography. *Cancer Res.* 2001;61:1781–1785.
14. Beer AJ, Haubner R, Goebel M, et al. Biodistribution and pharmacokinetics of the $\alpha_v\beta_3$ selective tracer ^{18}F galacto-RGD in cancer patients. *J Nucl Med.* 2005;46:1333–1341.
15. Beer AJ, Haubner R, Wolf I, et al. PET-based human dosimetry of ^{18}F-galacto-RGD, a new radiotracer for imaging alpha$_v$beta$_3$ expression. *J Nucl Med.* 2006;47:763–769.
16. Haubner R, Weber WA, Beer AJ, et al. Non-invasive visualization of the activated $\alpha_v\beta_3$ integrin in cancer patients by positron emission tomography and [^{18}F]galacto-RGD. *PLoS Med.* March 29, 2005 [Epub ahead of print].
17. Beer AJ, Haubner R, Sarbia M, et al. Positron emission tomography using [^{18}F]galacto-RGD identifies the level of integrin alpha$_v$beta$_3$ expression in man. *Clin Cancer Res.* 2006;12:3942–3949.
18. Haubner R, Kuhnast B, Mang C, et al. [^{18}F]Galacto-RGD: synthesis, radiolabeling, metabolic stability, and radiation dose estimates. *Bioconjug Chem.* 2004;15:61–69.
19. Brix G, Bellemann ME, Hauser H, et al. Recovery coefficients for the quantification of the arterial input functions from dynamic PET measurements: experimental and theoretical determination. *Nuklearmedizin.* 2002;41:184–190.
20. Bach-Gansmo T, Danielsson R, Saracco A, et al. Integrin receptor imaging of breast cancer: a proof-of-concept study to evaluate ^{99m}Tc-NC100692. *J Nucl Med.* 2006;47:1434–1439.

JNM The Journal of NUCLEAR MEDICINE

Patterns of $\alpha_v\beta_3$ Expression in Primary and Metastatic Human Breast Cancer as Shown by ^{18}F-Galacto-RGD PET

Ambros J. Beer, Markus Niemeyer, Janette Carlsen, Mario Sarbia, Jörg Nährig, Petra Watzlowik, Hans-Jürgen Wester, Nadia Harbeck and Markus Schwaiger

J Nucl Med. 2008;49:255-259.
Published online: January 16, 2008.
Doi: 10.2967/jnumed.107.045526

The Journal of Nuclear Medicine is published monthly.
SNMMI | Society of Nuclear Medicine and Molecular Imaging
1850 Samuel Morse Drive, Reston, VA 20190.
(Print ISSN: 0161-5505, Online ISSN: 2159-662X)

SNMMI SOCIETY OF NUCLEAR MEDICINE AND MOLECULAR IMAGING